Postbuckling of carbon nanotubes by atomic-scale finite element

A. Y. T. Leung,[a] X. Guo, and X. Q. He
Department of Building and Construction, City University of Hong Kong, Hong Kong

H. Jiang[b] and Y. Huang
Department of Mechanical and Industrial Engineering, University of Illinois at Urbana–Champaign, 1206 West Green Street, Urbana, Illinois 61801

(Received 3 August 2005; accepted 26 April 2006; published online 28 June 2006)

This paper employs an atomic-scale finite element method (AFEM) to study the postbuckling behavior of carbon nanotubes (CNTs). The computed energy curves and critical strain for the (8, 0) single-walled CNT (SWNT) agree well with atomistic simulations. The AFEM is very fast and versatile owing to the efficiency of the finite element method. For the SWNT, the strain energy curves have obvious jumps at morphology changes, and during the smooth continuation stages of postbuckling, the strain energy varies approximately linearly with the strain. For the double-walled CNT, there are only small strain energy releases, and the strain energy also changes approximately piecewise linearly with the strain. The morphologies are obtained in detail. AFEM is computationally fast and is an alternative efficient way to study the postbuckling of CNTs. © *2006 American Institute of Physics*. [DOI: 10.1063/1.2206607]

I. INTRODUCTION

Experimental investigation and theoretical research have displayed unique mechanical properties of carbon nanotubes (CNTs).[1–4] Large deformation of CNTs in the postbuckling stage was found in the atomic force microscope test of Falvo *et al.*[5] and the transmission electron microscopy test of Lourie *et al.*[6] Because there are few quantitative experimental results on their postbuckling characteristics, extensive theoretical research has been carried out to investigate their postbuckling behavior. In general, the widely used theoretical methods include atomistic based methods[7–11] and continuum mechanics.[12–17] Using molecular dynamics (MD), Yakobson *et al.*[7] found that single-walled CNT (SWNT) switches into different morphological patterns under large strain and that each shape change corresponds to an abrupt release of energy. Garg *et al.*[8] performed MD simulation on the interactions between proximal probe tips composed of CNTs and diamond, and between the probe tips and graphene surfaces. Liew *et al.*[11] studied the axial instability of SWNT and multiwalled CNTs (MWNTs). The atomistic based methods are currently far from predicting CNTs' behavior in large length and time scales, due to insufficient computing power.[11,18] Several elasticity models can be comparatively easily used. Ru[12] presented a shell model for the axial buckling of a double-walled CNT (DWNT). He *et al.*[13] established a shell buckling model based on the van der Waals (vdW) interaction between any two layers of MWNT. Pantano *et al.*[16] presented a structural mechanics model for the wrinkling study of MWNT. Shen[17] presented an elastic shell model for the postbuckling of DWNT subject to external hydrostatic pressure. In the above continuum models, the behavior of discrete atoms and concrete configuration of CNT in the postbuckling stage can hardly be achieved. Liu *et al.*[19,20] proposed an atomic-scale finite element method (AFEM). Using interatomic potential to consider the multibody interactions, AFEM is as accurate as molecular mechanics. It is much faster than molecular mechanics because it uses first and second order derivatives of total energy, while molecular mechanics employs the conjugate gradient method which only uses its first order derivative.

This paper employs AFEM to study the postbuckling behavior of CNTs. The achieved energy curves and critical strain for the (8, 0) SWNT agree well with the recent atomistic simulations. It is also found that the AFEM simulation employing the "second generation" empirical potential of Brenner *et al.*[21] is better than that employing Brenner's "first generation" empirical potential.[22] In the strain energy curves for the (7, 7) SWNT, there are obvious jumps at morphology changes. In the smooth continuation stages of postbuckling, the strain energy increases approximately linearly. Different results on the critical strains and the postbuckling characteristics are compared and discussed for two Brenner's potentials. For the DWNT, there are only small strain energy releases at morphology changes, and during each stage of postbuckling, the strain energy also varies approximately linearly with the strain. For the SWNT and DWNT in the postbuckling stages, their morphologies are presented in detail, and the different characteristics such as the strain energy and morphologies are compared.

II. POTENTIAL FUNCTION AND AFEM FOR CNTS

Using Brenner's potential,[21,22] the total potential energy U_{tot} stored in the atomic bonds of a CNT is expressed as

$$U_{\text{tot}} = \sum_{i=1}^{N} \sum_{j>i} (E_{ij}^{\text{REBO}} + E_{\text{vdW}}). \tag{1}$$

Here, N is the number of total atoms in the system and E_{vdW} is the energy due to vdW interaction. The interatomic forces

[a]Electronic mail: andrew.leung@cityu.edu.hk
[b]Present address: Department of Mechanical and Aerospace Engineering, Arizona State University, Tempe, Arizona 85287-6106.

are modeled according to the covalent bonding interactions

$$E_{ij}^{\mathrm{REBO}} = [V_R(r_{ij}) - b_{ij}V_A(r_{ij})], \tag{2}$$

where functions V_R and V_A are pair-additive interactions that represent all the interatomic repulsions (core-core, etc.) and attractions from valence electrons, respectively. The quantity r_{ij} is the distance between a pair of the nearest-neighbor atoms i and j, and b_{ij} is the reactive empirical bond order. Each carbon atom interacts with both the nearest- and second nearest-neighboring atoms, due to the dependence of the interatomic potential on bond length and bond angle. For a SWNT, the covalent bond among atoms is the dominant interaction. In the following simulation on the SWNT, vdW interaction is neglected. For a MWNT, vdW interaction is taken as a nonlinear spring when the distance between two carbon atoms is less than the cutoff radius. The total energy $E_{\mathrm{tot}}(x)$ is

$$E_{\mathrm{tot}}(x) = U_{\mathrm{tot}}(x) - \sum_{i=1}^{N} \bar{F}_i \cdot x_i, \tag{3}$$

where $x=(x_1,x_2,\ldots,x_N)^T$ is a vector of the positions of atoms, and $\bar{F}_i$ is the external force exerted on atom i.

In AFEM for CNTs proposed by Liu *et al.*,[19,20] an atomic-scale finite element consists of ten atoms because each carbon atom has three nearest-neighboring atoms and six second nearest-neighboring atoms. The associated element stiffness matrix and the nonequilibrium force vector are therein.[19,20] The number of nonzero entries in the global stiffness matrix K is of order N, so is the computational effort to solve $\mathrm{Ku}=P$.[19,20]

III. SIMULATION ON POSTBUCKLING OF CNTS

Consider an initial equilibrium configuration of CNT. One end of the CNT is fixed, and the in-plane displacements of the other end are prohibited. An axial displacement can be applied to compress it. The AFEM is performed to obtain its new equilibrium configuration. Then a further displacement is applied in small step. It deforms linearly when the strain is small. In the graph of average strain energy per atom versus strain, an equilibrium path representing linear deformation is extended until the stiffness matrix K loses positive definiteness.

After that, K is no longer positive definite, it is replaced by $K^*=K+\alpha I$, where I is the identity matrix and α is a positive number to ensure the positive definiteness of K^*.[19,20] A trial configuration is achieved by the AFEM. Based on the trial initial configuration, a new α is chosen to ensure the positive definiteness of the new K^*. We perform the AFEM calculation and replace the stiffness matrix repeatedly. The calculation will finally converge without replacing the stiffness matrix and a new point in the equilibrium path is found. The repeated replacement of stiffness matrix is an efficient way to obtain the modified initial configuration, and the final modified initial configuration may lead to a converged result. In the last step the replacement is not performed, so the final results will be the equilibrium configuration of the original system. Based on the new point, a new stable equilibrium path can be obtained. All calculation is performed by ABAQUS via its UEL (User-defined elements) subroutine.[23]

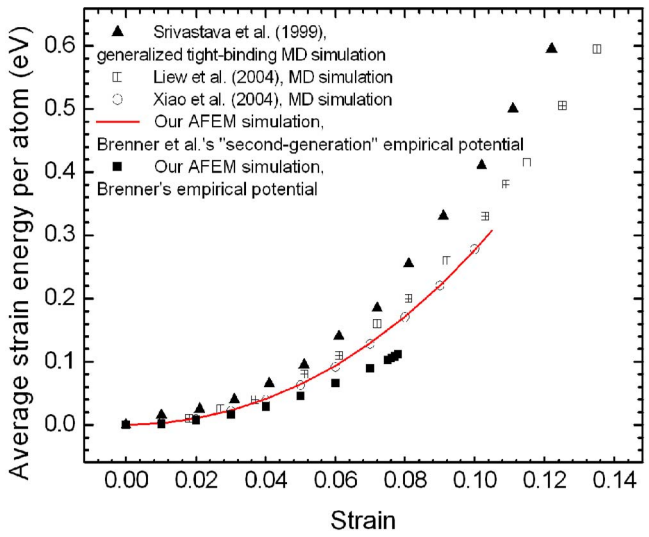

FIG. 1. Comparison among the curves of average strain energy for the (8, 0) SWNT.

A. Verification of AFEM

We use a (8,0) zigzag SWNT, with a length of 4.07 nm and a diameter of 0.63 nm, under axial compression as a first example. The average strain energy per atom is calculated as the difference in the average energy per atom in the strained and the unstrained states as a function of strain shown in Fig. 1. To show the effect of different potential on buckling, Brenner's first generation and second generation empirical potentials are employed. In Ref. 9, the structural deformation of the (8, 0) SWNT strained at 0.12 in the generalized tight-binding MD is completely spontaneous, leading to plastic collapse of the tube. Using the second generation empirical potential of Brenner *et al.*, Xiao *et al.*[10] investigated the axial instability of the SWNT by MD simulation and found that it can deform elastically up to a strain of 0.10. Liew *et al.*[11] performed MD simulation on a (8, 0) SWNT also using the second generation empirical potential of Brenner *et al.* and showed that it can be compressed up to a strain of 0.135 before buckling. In our calculation, when the second generation empirical potential of Brenner *et al.* is employed, the critical strain is 0.105; when Brenner's first generation empirical potential is employed, the critical strain is 0.078. The strain energy curves of Srivastava *et al.*, Xiao *et al.*, and Liew *et al.* are compared in Fig. 1. It can be easily observed that our energy curve approaches theirs closely. The energy curves of Xiao *et al.* and ours based on the second generation empirical potential of Brenner *et al.* are almost coincident. Srivastava *et al.* achieved the highest strain energy using the generalized tight-binding MD scheme of Menon *et al.*,[24] the simulations based on which are in good agreement with experimental results for the structural and vibrational properties of CNTs. Judging from the energy curve and the critical strain of Srivastava *et al.*, our AFEM simulation based on the second generation empirical potential of Brenner *et al.* is better than that based on Brenner's first generation empirical

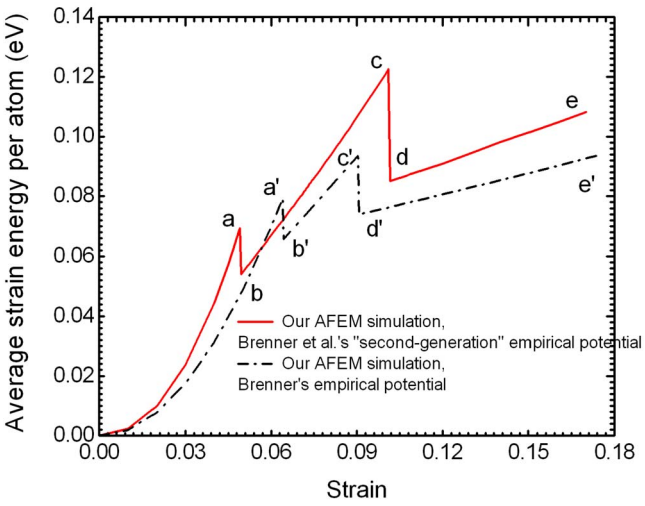

FIG. 2. The curve of average strain energy for the (7, 7) SWNT when both Brenner's potentials are employed.

potential. The time needed really depends on the control parameters such as the applied total displacement step size and the initial step size. In this simulation, only tens of seconds are needed to achieve the final critical strain.

B. Simulation results on postbuckling of SWNT

We study a (7, 7) armchair SWNT, with a length of 6 nm and a diameter of 0.95 nm, under axial compression to study its postbuckling behavior. Both Brenner's potentials are employed, and the two associated energy curves are presented in Fig. 2 to show the effect of different Brenner's potential on the characteristics of postbuckling behaviors. The strain energy obviously jumps at morphology changes in the macrocontinuum mechanics.[25,26] Our current research shows that the energy curves of the SWNT have the same feature. In the energy curves of Yakobson *et al.*[7] and Iijima *et al.*[27] by MD simulation, there are abrupt releases of energy, while in our energy curves, there are always two obvious jumps corresponding to abrupt morphologic changes.

When the second generation empirical potential of Brenner *et al.* is employed, the morphologies of SWNT at each characteristic strain are shown in Fig. 3.[28] In the postbuckling stages, its morphologies are not axis symmetric. For illustration, we present them in two perpendicular directions. At small strains, it deforms linearly and keeps straight in Fig. 3(a). The strain energy grows parabolically as shown in the part from the origin to point *a* in Fig. 2, until the critical strain of 0.0492. After that, the strain energy drops about 22%, and it enters into the postbuckling stage. At the beginning of this stage, Fig. 3(b) shows three perpendicular flattenings. With increasing strain, the central fin becomes flatter and narrower in Fig. 3(c). From point *b* to *c* in Fig. 2, the strain energy increases approximately linearly until the second critical strain of 0.101. Then the strain energy drops about 30.5% to another straight line and increases again. The flattening corresponds to a hinge in Fig. 3(d), similar to that of Yakobson *et al.*[7] In their work it is squashed entirely at a

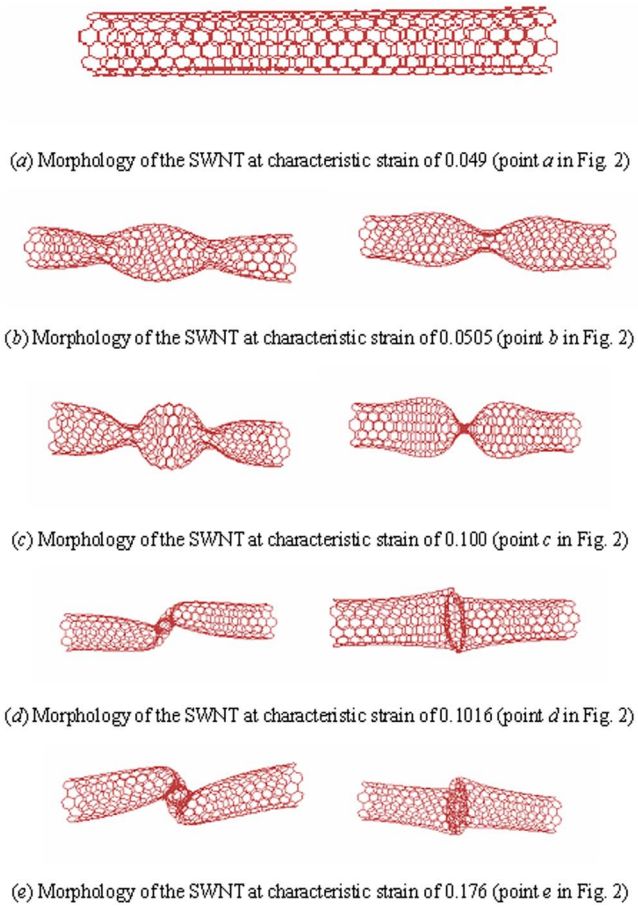

FIG. 3. The morphologies of (7, 7) SWNT at each characteristic strain when Brenner's "second generation" empirical potential is employed. In the postbuckling stages (b)–(e), they are presented in two perpendicular directions. (a) Morphology of the SWNT at a characteristic strain of 0.049 (point *a* in Fig. 2). (b) Morphology of the SWNT at a characteristic strain of 0.0505 (point *b* in Fig. 2). (c) Morphology of the SWNT at a characteristic strain of 0.100 (point *c* in Fig. 2). (d) Morphology of the SWNT at a characteristic strain of 0.1016 (point *d* in Fig. 2). (e) Morphology of the SWNT at a characteristic strain of 0.176 (point *e* in Fig. 2).

strain of 0.13, while in our simulation, it can deform steadily, with only its central part being squashed, until the strain of 0.17 in Fig. 3(e).

When Brenner's first generation empirical potential is employed, similar to the former case, the energy curve has one linear deformation stage and two postbuckling stages. Its morphologies at each characteristic strain are nearly the same as those in the former case. The critical strain is 0.064. Liu *et al.*[19,20] also showed that it is between 0.06 and 0.07. Then the strain energy drops about 17.2% and it enters into the postbuckling stage where it also displays three flattenings. The second critical strain is 0.904, and the strain energy drops about 20.9% to another straight line and increases again. The flattening works as a hinge, too. It can deform steadily until the strain of 0.174.

In the linear stages shown in Fig. 2, the energy when the second generation empirical potential of Brenner *et al.* is employed is always larger than that when Brenner's first generation empirical potential is employed. In each case, it is found in Fig. 2 that in the postbuckling stages the energy changes approximately linearly with strain, in agreement

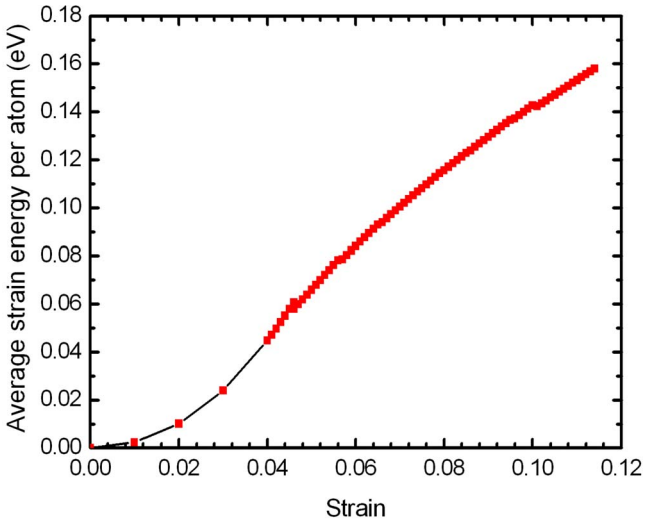

FIG. 4. The curve of average strain energy of the (5, 5) and (10, 10) DWNT when the "second generation" empirical potential of Brenner *et al.* is employed.

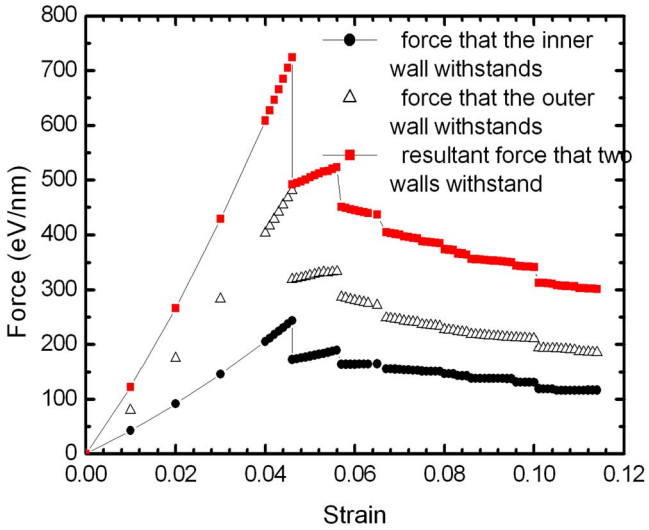

FIG. 5. The forces suffered by the inner and outer walls, respectively, and their resultant via the strain for the (5, 5) and (10, 10) DWNT.

with Yakobson *et al.*[7] and Liew *et al.*[11] There are always obvious drops at critical points in the energy curve, consistent with the recent research.[11] In each case, due to two obvious energy drops, our maximum strain energy is much smaller than that of Yakobson *et al.*[7] For each curve, the slope of the straight line in the second stage of postbuckling is smaller than that in the first stage of postbuckling. When the second-generation empirical potential of Brenner *et al.* is employed, the critical strain is smaller, while the second critical strain is larger, and the slope of the straight line is larger in the two stages of postbuckling, respectively.

C. Simulation results on postbuckling of DWNT

The second-generation empirical potential of Brenner *et al.* is employed to study postbuckling behavior of (5, 5) and (10, 10) DWNT, with a length of 6.0 nm and a diameter of 1.356 nm. The strain energy curve is shown in Fig. 4. The critical strain is 0.046, where the strain energy is 0.061 eV and then drops 4.6%. The strain energy curve has one linear deformation stage and many postbuckling stages, and there are only small energy releases at morphology changes, while in the case of SWNT, the strain energy can drop 10%–30% at morphology changes. In each postbuckling stage, the strain energy increases approximately linearly, and the slope of the latter line section is smaller than that of the former one, consistent with the simulation on the SWNT. Because there is no large energy drops, the final strain energy at the strain of 0.11 is 2.6 times that at the critical strain.

Forces that the inner wall and the outer wall withstand are shown in Fig. 5 as a function of the strain. Before the buckling, two forces increase very fast and approximately linearly, and the latter is almost twice of the former. At the critical strain, the force that the inner wall withstands decreases 29.3%, and the force that the outer wall withstands decreases 33.5%. In the first stage of postbuckling, two forces increase.

In the second stage of the postbuckling, the force that the inner wall withstands increases slowly while that the outer wall withstands decreases slowly. In the following stages, two forces decrease very slowly. When the strain is 0.114, the force the inner wall withstands is 116.6 eV/nm, while the force the outer wall withstands is 185.1 eV/nm, and the latter is 1.59 times of the former. During the postbuckling, the mechanism on how the applied load is distributed to the two walls of DWNT is changing with the configuration. The resultant force that two walls of the DWNT withstand is also shown in Fig. 5. Similarly, before the buckling, the force increases very fast and approximately linearly. At the critical strain, it decreases 32.1%. The force increases with the strain in the first stage of the postbuckling and then decreases very slowly.

The morphologies at the strains of 0.05, 0.07, 0.09, and 0.11 are shown in Fig. 6 in two perpendicular directions.[28] Similar to the SWNT, the morphologies of both the inner and outer tubes of the DWNT are not axis symmetric. Due to the complex vdW interaction between two walls, its morphologies are much more complicated than those of the SWNT (7, 7) though they have the nearly identical length. At the strain of 0.05, it contains two perpendicular flattenings, as shown in Fig. 6(a). At the strains of 0.07, 0.09, and 0.11, it contains five perpendicular flattenings, as shown in Figs. 6(b)–6(d). With the strain increasing, the flattenings also become flatter and narrower. At the strain of 0.11, the inner wall is almost squashed. When the strain is very large, for the SWNT, the central flattening behaves like a hinge, while for the DWNT, the flattening still does not behave like a hinge at the strain of 0.11.

IV. CONCLUSIONS

This paper employs the AFEM to study the postbuckling of CNTs. The energy curves and critical strain for the (8, 0) SWNT verify the application of the AFEM. Whether Brenner's or the "second-generation" empirical potential of Brenner *et al.* is adopted, the energy curve of SWNT always has

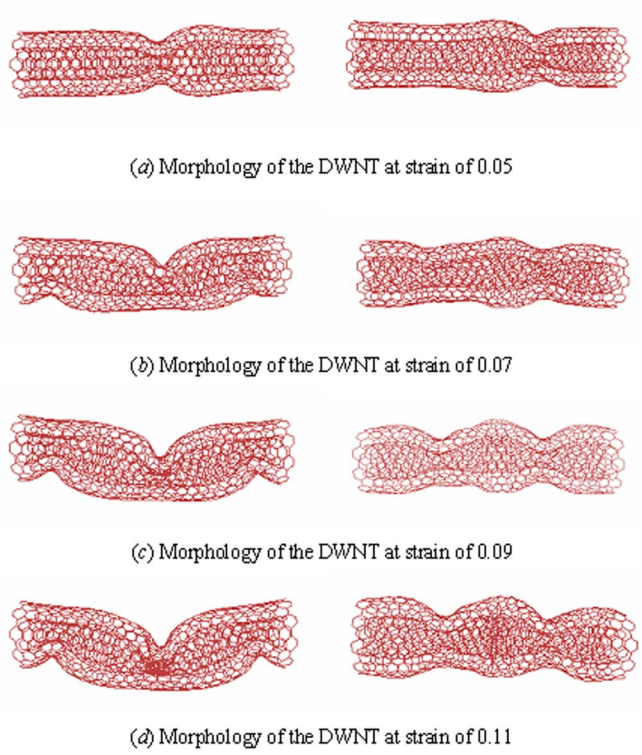

FIG. 6. The morphologies of the (5, 5) and (10, 10) DWNT when the "second generation" empirical potential of Brenner *et al.* is employed. They are presented in two perpendicular directions. (a) Morphology of the DWNT at a strain of 0.05. (b) Morphology of the DWNT at a strain of 0.07. (c) Morphology of the DWNT at a strain of 0.09. (d) Morphology of the DWNT at a strain of 0.11.

one linear deformation stage and several postbuckling stages, and there are obvious jumps at morphology changes. In the smooth postbuckling stages, the strain energy increases approximately linearly with the strain. For the DWNT, the strain energy has comparatively small drops, and during each stage of postbuckling, it also changes approximately linearly with the strain. For the SWNT and DWNT in the postbuckling stages, their morphologies are illustrated in detail, and the different characteristics such as the strain energy and morphologies are compared. The AFEM is very fast and versatile owing to the efficiency of the finite element method.

ACKNOWLEDGMENT

The research is supported by City University of Hong Kong Grant No. SRG7001824.

[1] M. M. J. Treacy, T. W. Ebbesen, and J. M. Gibson, Nature (London) **381**, 678 (1996).
[2] E. W. Wong, P. E. Sheehan, and C. M. Lieber, Science **277**, 1971 (1997).
[3] D. Qian, G. J. Wagner, W. K. Liu, M. F. Yu, and R. S. Ruoff, Appl. Mech. Rev. **55**, 495 (2002).
[4] Y. Huang and Z. L. Wang, in *Comprehensive Structural Integrity Handbook*, edited by B. Karihaloo, R. Ritchie, and I. Milne (Elsevier, Amsterdam, 2003), Vol. 8, p. 551.
[5] M. R. Falvo, G. J. Clary, R. M. Taylor II, V. Chi, F. P. Brooks Jr., S. Washburn, and R. Superfine, Nature (London) **389**, 582 (1997).
[6] O. Lourie, D. M. Cox, and H. D. Wagner, Phys. Rev. Lett. **81**, 1638 (1998).
[7] B. I. Yakobson, C. J. Brabec, and J. Bernholc, Phys. Rev. Lett. **76**, 2511 (1996).
[8] A. Garg, J. Han, and S. B. Sinnott, Phys. Rev. Lett. **81**, 2260 (1998).
[9] D. Srivastava, M. Menon, and K. Cho, Phys. Rev. Lett. **83**, 2973 (1999).
[10] T. Xiao, X. Xu, and K. Liao, J. Appl. Phys. **95**, 8145 (2004).
[11] K. M. Liew, C. H. Wong, X. Q. He, M. J. Tan, and S. A. Meguid, Phys. Rev. B **69**, 115429 (2004).
[12] C. Q. Ru, Phys. Rev. B **62**, 16962 (2000).
[13] X. Q. He, S. Kitipornchai, and K. M. Liew, J. Mech. Phys. Solids **53**, 303 (2005).
[14] C. Y. Li and T. W. Chou, Mech. Mater. **36**, 1047 (2004).
[15] T. C. Chang, G. Q. Li, and X. M. Guo, Carbon **43**, 287 (2005).
[16] A. Pantano, D. M. Parks, and M. C. Boyce, J. Mech. Phys. Solids **52**, 789 (2004).
[17] H. S. Shen, Int. J. Solids Struct. **41**, 2643 (2004).
[18] K. M. Liew, X. Q. He, and C. H. Wong, Acta Mater. **52**, 2521 (2004).
[19] B. Liu, Y. Huang, H. Jiang, S. Qu, and K. C. Hwang, Comput. Methods Appl. Mech. Eng. **193**, 1849 (2004).
[20] B. Liu, H. Jiang, Y. Huang, S. Qu, M. F. Yu, and K. C. Hwang, Phys. Rev. B **72**, 035435 (2005).
[21] D. W. Brenner, O. A. Shenderova, J. A. Harrison, S. J. Stuart, B. Ni, and S. B. Sinnott, J. Phys.: Condens. Matter **14**, 783 (2002).
[22] D. W. Brenner, Phys. Rev. B **42**, 9458 (1990).
[23] ABAQUS, ABAQUS Theory Manual and Users Manual, version 6.5, Hibbit, Karlsson and Sorensen, Pawtucket, RI, 2005.
[24] M. Menon, E. Richter, and K. R. Subbaswamy, J. Chem. Phys. **104**, 5875 (1996).
[25] Z. P. Bazant and L. Cedolin, *Stability of Structures* (Oxford University Press, Oxford, 1991).
[26] Z. Waszczyszyn, C. Cichon, and M. Radwanska, *Stability of Structures by finite Element Methods* (Elsevier, New York, 1994).
[27] S. Iijima, C. Brabec, A. Maiti, and J. Bernholc, J. Chem. Phys. **104**, 2089 (1996).
[28] W. Humphrey, A. Dalke, and K. Schulten, J. Mol. Graphics **14**, 33 (1996).